

Few-Qubit Lasing in Circuit QED

Stephan André^{1,4}, Valentina Brosco², Michael Marthaler^{1,4},
Alexander Shnirman^{3,4}, Gerd Schön^{1,4}

¹Institut für Theoretische Festkörperphysik, Universität Karlsruhe, 76128 Karlsruhe, Germany

²Dipartimento di Fisica, Università “La Sapienza”, P.le A. Moro 2, 00185 Roma, Italy

³Institut für Theorie der Kondensierten Materie, Universität Karlsruhe, 76128 Karlsruhe, Germany

⁴DFG Center for Functional Nanostructures (CFN), Universität Karlsruhe, 76128 Karlsruhe, Germany

E-mail: schoen@kit.edu

Abstract. Motivated by recent experiments, which demonstrated lasing and cooling of the electromagnetic modes in a resonator coupled to a superconducting qubit, we describe the specific mechanisms creating the population inversion, and we study the spectral properties of these systems in the lasing state. Different levels of the theoretical description, i.e., the semi-classical and the semi-quantum approximation, as well as an analysis based on the full Liouville equation are compared. We extend the usual quantum optics description to account for strong qubit-resonator coupling and include the effects of low-frequency noise. Beyond the lasing transition we find for a single- or few-qubit system the phase diffusion strength to grow with the coupling strength, which in turn deteriorates the lasing state. This may lead to a double peak structure of the power spectrum.

PACS numbers: 85.25.Cp 42.50.Pq 03.65.Yz

1. Introduction

The search for efficient coupling and read-out architectures of scalable solid-state quantum computing systems has opened a new field, called “circuit QED” [1].

Circuit QED is the analogue on chip of quantum optics “cavity QED” where superconducting qubits play the role of (artificial) atoms and an electromagnetic resonator replaces the cavity. The resonators can be used to read out the qubit state [2, 3, 4, 5] or to couple qubits to perform single- and two-qubit gates [6, 7, 8, 9].

Apart from such applications for quantum information processing, circuit QED offers the possibility to study quantum optics effects in electrical circuits: Fock states of the electromagnetic field were created and detected [10], and the coherent control of photon propagation via electromagnetically induced transparency was shown [11]. In addition lasing and cooling of the electromagnetic field in the resonator has been demonstrated: By creating a population inversion in a driven superconducting single-electron transistor (SSET) coupled capacitively to a microstripline resonator, Astafiev *et al.* [12] could excite a lasing peak in the spectrum. In another experiment, Grajcar *et al.* [13] coupled a driven flux qubit to a low-frequency LC resonator and observed both cooling and a tendency towards lasing via the so-called Sisyphus mechanism.

In contrast to conventional lasers where many atoms are coupled weakly to the light field in a Fabry-Perot cavity, in the micromasers realized, e.g., in Refs. [12, 13] a single superconducting qubit is coupled strongly to the microwave field in the resonator. Compared to conventional lasers one expects for single-atom lasers a lower intensity of the radiation but stronger fluctuation effects. Specifically, the quantum fluctuations of the photon number associated with spontaneous emission, which are known to lead to the *phase diffusion* of the laser field [14], have more pronounced consequences. As a result, even in the lasing state, phase coherence is lost after a characteristic time τ_d , which sets a limit on the linewidth of the laser radiation and thus on the visibility of the lasing signal. Phase diffusion was observed experimentally in a single-qubit maser in Ref. [12]; the dependence of the phase diffusion on the coupling strength was analyzed theoretically by the present authors in Ref. [15].

In the present work we analyze the static and spectral properties of single- and few-qubit lasers, focusing on the regime of strong qubit-resonator coupling realized in most circuit QED experiments. Using a Master equation approach we analyze the consequences of qubit-field correlations and, in the case of few-qubit lasing, we evaluate the corrections due to qubit-qubit correlations. We show that, in the strong coupling regime, qubit-field correlations may have significant quantitative effects on the laser line-width. On the other hand, the qubit-qubit correlations, which are strongest at the transition to the lasing regime, yield only small corrections to the power spectrum. In the frame of the so-called “semi-quantum” approximation [16] we describe the qualitative differences between multi-atom lasers and superconducting micromasers; specifically we analyze the scaling of the lasing transition and diffusion constant with the number of atoms.

The paper is organized as follows.

We start discussing in the following Section the two experimental realizations of superconducting micromasers reported in Refs. [12] and [2, 13], respectively. In particular we describe how the population inversion in the qubit is created in the two examples. In Section 3, we formulate the theoretical model and derive the dynamical equations for the micromaser. Both quantum Langevin equations and the master equation are presented. In Section 4 we review the theory of lasing, paying attention to effects which are usually ignored for conventional lasers but are prominent in single- or few-atom lasers in the strong coupling regime. We introduce the different approximation schemes. Static properties of single-qubit lasers are presented, such as the average photon number and the qubit-field and qubit-qubit correlations. We show explicitly that due to spontaneous emission in few-qubit lasers the sharp lasing threshold is replaced by a smooth, but still well localized transition to the lasing regime.

Next, in section 5, we analyze the spectral properties of superconducting micromasers and relate the phase diffusion of the resonator field to the average photon number and the qubit inversion. We discuss the effects of correlations between qubit and resonator on the diffusion process and we show how the interplay between strong coupling and spontaneous emission may lead to a double peak structure in the spectrum. Finally, in section 6 we analyze the scaling of the photon number and of the diffusion constant with the number of atoms. In addition we demonstrate how low-frequency noise leads to inhomogeneous broadening of the lasing peak.

2. Inversion mechanisms in superconducting micromasers

2.1. The SSET laser

The “SSET laser” realized by Astafiev *et al.* [12] consists of a superconducting single-electron transistor coupled capacitively to a microstripline resonator, as shown in Fig. 1a. The properties of the coupled system and the specific form of the Hamiltonian will be analyzed further in later Sections and in Appendix A. In the present Section we describe how a population inversion is created in a suitably biased SSET.

A superconducting single-electron transistor (SSET) consists of two superconducting leads coupled by tunnel junctions to a superconducting island. A gate voltage U shifts the electrostatic energy of the island and controls, together with the bias voltage V , the current through the device. The Josephson coupling, E_J , allowing for coherent Cooper pair tunneling through the junctions, is weak compared to the superconducting energy gap Δ_{sc} and to the charging energy of the island, $E_C = e^2/2C$, C being the total island’s capacitance. In addition, quasiparticles can tunnel incoherently (with rate $\propto V/eR$, where R is the resistance of the tunnel junction) when the energy difference between initial and final states is sufficient to create a quasiparticle excitation, i.e., when it exceeds twice the gap, $|\Delta E| \geq 2\Delta_{sc}$. We denote by N the number of excess charges on the island; it changes by ± 1 in a single-electron tunneling process and by ± 2 in a

Cooper pair tunneling event. At low temperatures for the conditions realized experimentally the number of accessible charge states of the island is strongly reduced. For the further calculations we can restrict our analysis to $N = 0, 1, 2$.

We assume the SSET to be tuned close to the Josephson quasiparticle (JQP) cycle, where the current is transported by a combination of Cooper pair tunneling through one junction and two consecutive quasiparticle tunneling events through the other junction. The parameters of the junctions are chosen asymmetrically. By changing the transport voltage V and the gate voltage U , we can tune to a situation, where resonant Cooper pair tunneling is strong across, say, the lower junction, while quasiparticle tunneling is strong across the upper one. Specifically, when the normalized “gate charge” $N_G = C_G U/e$ is approximately 1, $N_G \approx 1$, the charge states $|N = 0\rangle$ and $|N = 2\rangle$ are near degeneracy with respect to coherent Cooper pair tunneling across the lower junction. Hence the eigenstates are

$$\begin{aligned} |\uparrow\rangle &= \cos \frac{\xi}{2} |N = 0\rangle + \sin \frac{\xi}{2} |N = 2\rangle \\ |\downarrow\rangle &= \sin \frac{\xi}{2} |N = 0\rangle - \cos \frac{\xi}{2} |N = 2\rangle \end{aligned} \quad (1)$$

where $\tan \xi = E_J/\epsilon_{ch}$ with $\epsilon_{ch} = 4(N_G - 1)E_C$. Quasiparticle tunneling across the upper

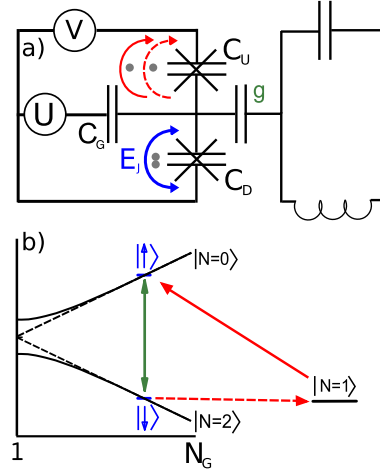


Figure 1. a) The SSET consist of two superconducting leads coupled to an island via Josephson junctions with capacitance C_U and C_D . A transport voltage V is applied, and the electrostatic energy of the island is tuned by the gate voltage U via the capacitance C_G . In addition, the SSET is capacitively coupled to an LC-oscillator with strength g .

b) Energies of the charge states $|N = 0\rangle$ and $|N = 2\rangle$ (dashed lines) and the eigenstates $|\uparrow\rangle$ and $|\downarrow\rangle$ (full lines). The energy of the odd charge state $|N = 1\rangle$ may be far from the other ones and is drawn at an arbitrary position. If the charge states $|N = 0\rangle$ and $|N = 2\rangle$ are not close to degeneracy, Cooper pair tunneling is suppressed. For $N_G > 1$ we have $\cos \frac{\xi}{2} > \sin \frac{\xi}{2}$, and the dominant quasiparticle transitions lead from $|\downarrow\rangle$ to $|\uparrow\rangle$, as indicated by the red arrows. The capacitive coupling to the LC-oscillator creates an additional coupling between the states $|\uparrow\rangle$ and $|\downarrow\rangle$, indicated by the green arrow.

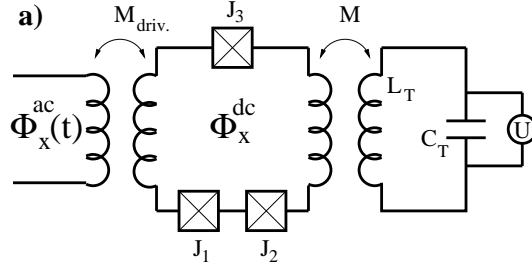


Figure 2. In the setup of Ref. [2] an externally driven three-junction flux qubit is coupled inductively to an LC oscillator.

junction leads to transitions between the states $|\uparrow\rangle$ and $|\downarrow\rangle$ and the odd charge state $|N=1\rangle$. The transition rates are

$$\begin{aligned}\Gamma_{\downarrow\rightarrow 1} &= \Gamma_{1\rightarrow\uparrow} = \cos^2\left(\frac{\xi}{2}\right) I(V) \\ \Gamma_{\uparrow\rightarrow 1} &= \Gamma_{1\rightarrow\downarrow} = \sin^2\left(\frac{\xi}{2}\right) I(V).\end{aligned}\quad (2)$$

The dependence on the relevant matrix elements and the energy gain eV can be lumped into the function $I(V)$, which is the normal current through the junction at voltage V . Here we can assume that the relevant energy scale for each tunnel event is the applied voltage and neglect the smaller change of the energy of the island.

By choosing ξ such that $\cos \frac{\xi}{2} > \sin \frac{\xi}{2}$, we can create a population inversion. In this case, the quasiparticle tunneling processes (2) leading from $|\downarrow\rangle$ via $|1\rangle$ to $|\uparrow\rangle$ become stronger than the processes in opposite direction (see fig. 1b)). From the transition rates (2) we readily obtain the bare population inversion in the system,

$$D_0 = \frac{\rho_{\uparrow\uparrow} - \rho_{\downarrow\downarrow}}{\rho_{\uparrow\uparrow} + \rho_{\downarrow\downarrow}} = \cos \xi \quad (3)$$

where ρ_{ii} is the population of the state $|i\rangle$ with $i = \uparrow, \downarrow$.

2.2. The superconducting dressed-state laser

In this subsection we consider systems as investigated in Ref. [2, 13] and shown in Fig. 2. Here, a flux qubit is strongly driven by *ac*-fields to perform Rabi oscillations. It is further coupled to a low-frequency *LC*-oscillator. In the strongly driven situation the physics is most conveniently described in the basis of “dressed states” in the rotating frame [17]. The transformation to dressed states modifies the relaxation, excitation and decoherence rates as compared to the standard results [18, 19]. As a result, for blue detuning of the driving frequency compared to the resonant frequency a population inversion is produced in the dressed state basis, which in turn can lead to lasing [20].

To illustrate these effects we first consider the driven qubit (ignoring the coupling to the resonator) coupled to a bath observable \hat{X} ,

$$H = -\frac{1}{2} \Delta E \sigma_z + \hbar \Omega_{R0} \cos(\omega_d t) \sigma_x$$

$$-\frac{1}{2}(b_x\sigma_x + b_y\sigma_y + b_z\sigma_z)\hat{X} + H_{\text{bath}}. \quad (4)$$

In the absence of driving, $\Omega_{R0} = 0$, and for regular (i.e., smooth as function of the frequency) power spectra of the fluctuating bath observables we can proceed using Golden rule type arguments [18, 19]. The transverse noise, coupling to σ_x and σ_y , is responsible for relaxation and excitation processes with rates

$$\begin{aligned} \Gamma_{\downarrow} &= \frac{|b_{\perp}|^2}{4\hbar^2} \langle \hat{X}^2 \rangle_{\omega=\Delta E} \\ \Gamma_{\uparrow} &= \frac{|b_{\perp}|^2}{4\hbar^2} \langle \hat{X}^2 \rangle_{\omega=-\Delta E}, \end{aligned} \quad (5)$$

while longitudinal noise, coupling to σ_z , produces a pure dephasing with rate

$$\Gamma_{\varphi}^* = \frac{|b_z|^2}{2\hbar^2} S_X(\omega = 0). \quad (6)$$

Here $b_{\perp} \equiv b_x + ib_y$, and we introduced the ordered correlation function $\langle \hat{X}^2 \rangle_{\omega} \equiv \int dt e^{i\omega t} \langle \hat{X}(t)\hat{X}(0) \rangle$, as well as the power spectrum, i.e., the symmetrized correlation function, $S_X(\omega) \equiv (\langle \hat{X}^2 \rangle_{\omega} + \langle \hat{X}^2 \rangle_{-\omega})/2$. The rates (5) and (6) also define the relaxation rate $1/T_1 = \Gamma_1 = \Gamma_{\downarrow} + \Gamma_{\uparrow}$ and the total dephasing rate $1/T_2 = \Gamma_{\varphi} = \Gamma_1/2 + \Gamma_{\varphi}^*$ which appear in the Bloch equations for the qubit.

To account for the driving with frequency ω_d it is convenient to transform to the rotating frame via a unitary transformation $U_r = \exp(-i\omega_d \sigma_z t/2)$. Within RWA the transformed Hamiltonian reduces to

$$\begin{aligned} \tilde{H} &= \frac{1}{2}\hbar\Omega_{R0}\sigma_x + \frac{1}{2}\hbar\delta\omega\sigma_z \\ &\quad - \frac{1}{2}[b_z\sigma_z + b_{\perp}e^{i\omega_d t}\sigma_{-} + b_{\perp}^*e^{-i\omega_d t}\sigma_{+}]\hat{X} + H_{\text{bath}}, \end{aligned} \quad (7)$$

with detuning $\delta\omega \equiv \omega_d - \Delta E/\hbar$. The RWA cannot be used in the second line of (7) since the fluctuations \hat{X} contain potentially frequencies close to $\pm\omega_d$, which can compensate fast oscillations. Diagonalizing the first two terms of (7) one obtains

$$\begin{aligned} \tilde{H} &= \frac{1}{2}\hbar\Omega_R\sigma_z + H_{\text{bath}} \\ &\quad - \left[\frac{\sin\beta}{2}b_z + \frac{\cos\beta}{4}(b_{\perp}^*e^{-i\omega_d t} + b_{\perp}e^{i\omega_d t}) \right] \sigma_z \hat{X} \\ &\quad - \left\{ \left[\frac{\sin\beta+1}{4}b_{\perp}^*e^{-i\omega_d t} + \frac{\sin\beta-1}{4}b_{\perp}e^{i\omega_d t} - \frac{\cos\beta}{2}b_z \right] \sigma_{+} \hat{X} + \text{h.c.} \right\}, \end{aligned} \quad (8)$$

where the full Rabi frequency is $\Omega_R = \sqrt{\Omega_{R0}^2 + \delta\omega^2}$, and the detuning determines the parameter β via

$$\tan\beta = \delta\omega/\Omega_{R0}. \quad (9)$$

From here Golden-rule arguments lead to the relaxation and excitation rates in the rotating frame as well as the "pure" dephasing rate [21]

$$\tilde{\Gamma}_{\downarrow} \approx \frac{b_z^2}{4\hbar^2} \cos^2\beta \langle \hat{X}^2 \rangle_{\Omega_R}$$

$$\begin{aligned}
& + \frac{|b_\perp|^2}{16\hbar^2} \left[(1 - \sin \beta)^2 \langle \hat{X}^2 \rangle_{\omega_d + \Omega_R} + (1 + \sin \beta)^2 \langle \hat{X}^2 \rangle_{-\omega_d + \Omega_R} \right] \\
\tilde{\Gamma}_\uparrow & \approx \frac{b_z^2}{4\hbar^2} \cos^2 \beta \langle \hat{X}^2 \rangle_{-\Omega_R} \\
& + \frac{|b_\perp|^2}{16\hbar^2} \left[(1 - \sin \beta)^2 \langle \hat{X}^2 \rangle_{-\omega_d - \Omega_R} + (1 + \sin \beta)^2 \langle \hat{X}^2 \rangle_{\omega_d - \Omega_R} \right] , \\
\tilde{\Gamma}_\varphi^* & \approx \frac{b_z^2}{2\hbar^2} \sin^2 \beta S_X(\omega = 0) + \frac{|b_\perp|^2}{4\hbar^2} \cos^2 \beta S_X(\omega_d).
\end{aligned} \tag{10}$$

We note the effect of the frequency mixing. In addition, due to the diagonalization the effects of longitudinal and transverse noise on relaxation and decoherence get mixed. We further note that the rates also depend on the fluctuations' power spectrum at the Rabi frequency, $\langle \hat{X}^2 \rangle_{\pm\Omega_R}$.

For a sufficiently regular power spectrum of the fluctuations at frequencies $\omega \approx \pm\Delta E/\hbar$ we can ignore the effect of detuning and the small shifts by $\pm\Omega_R$ as compared to the high frequency $\omega_d \approx \Delta E/\hbar$. We further assume that $\Omega_R \ll kT/\hbar$. In this case we find the simple relations

$$\begin{aligned}
\tilde{\Gamma}_\uparrow & = \frac{(1 + \sin \beta)^2}{4} \Gamma_\downarrow + \frac{(1 - \sin \beta)^2}{4} \Gamma_\uparrow + \frac{1}{2} \cos^2 \beta \Gamma_\nu , \\
\tilde{\Gamma}_\downarrow & = \frac{(1 - \sin \beta)^2}{4} \Gamma_\downarrow + \frac{(1 + \sin \beta)^2}{4} \Gamma_\uparrow + \frac{1}{2} \cos^2 \beta \Gamma_\nu , \\
\tilde{\Gamma}_\varphi^* & = \sin^2 \beta \Gamma_\varphi^* + \frac{\cos^2 \beta}{2} (\Gamma_\downarrow + \Gamma_\uparrow) ,
\end{aligned} \tag{11}$$

where the rates in the lab frame are given by Eqs. (5,6) and the new rate

$$\Gamma_\nu \equiv \frac{1}{2\hbar^2} b_z^2 S_X(\Omega_R) \tag{12}$$

depends on the power spectrum at the Rabi frequency.

To proceed we concentrate on the most relevant regime. At low temperatures, $k_B T \ll \Delta E \approx \hbar\omega_d$, we can neglect Γ_\uparrow as it is exponentially small. We also assume that Γ_ν can be neglected as compared to Γ_\downarrow , which is justified, e.g., when the qubit is tuned close to the symmetry point where $b_z \ll |b_\perp|$. Since the rate Γ_ν depends on the noise power spectrum at the frequency Ω_R , which is usually higher than the frequency range of the $1/f$ noise, the latter does not change the situation. Thus we neglect Γ_ν and we are left with

$$\tilde{\Gamma}_{\downarrow/\uparrow} \approx \frac{(1 \mp \sin \beta)^2}{4} \Gamma_\downarrow , \quad \tilde{\Gamma}_\varphi^* \approx \frac{\cos^2 \beta}{2} \Gamma_\downarrow . \tag{13}$$

The ratio of up- and down-transitions depends on the detuning and can be expressed by an effective temperature. Right on resonance, where $\beta = 0$, we have $\tilde{\Gamma}_\uparrow = \tilde{\Gamma}_\downarrow$, corresponding to infinite temperature or a classical drive. For “blue” detuning, $\beta > 0$, we find $\tilde{\Gamma}_\uparrow > \tilde{\Gamma}_\downarrow$, i.e., *negative temperature*. This leads to a population inversion of the qubit, which is the basis for the lasing behavior which will be described below.

In a more careful analysis, paying attention to the small frequency shifts by $\pm\Omega_R$,

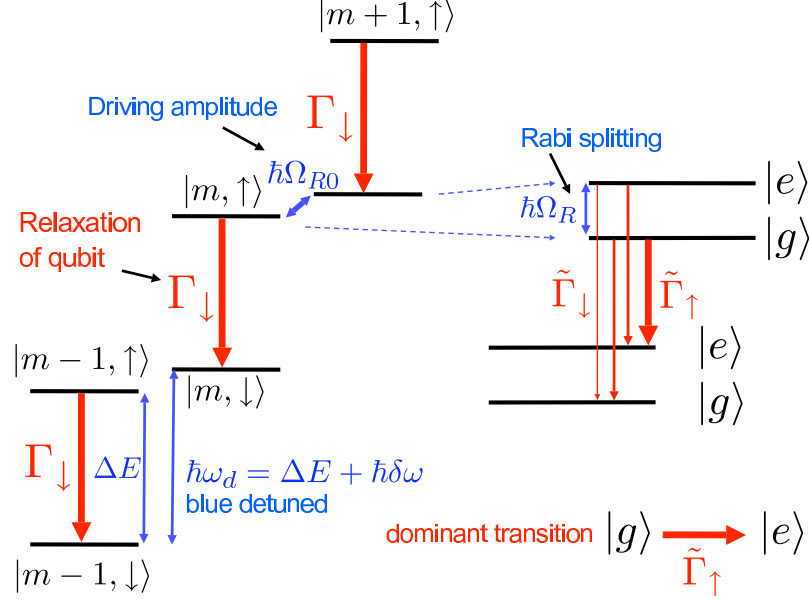


Figure 3. Relaxation rates in the basis of the dressed states. The left staircase denotes the eigenstates of the undriven qubit, $|\uparrow\rangle, |\downarrow\rangle$ and the (quantized) driving field, $|m\rangle$, before the driving is switched on, i.e., for $\Omega_{R0} = 0$. The Hamiltonian in this basis is obtained from (4) by replacing $\hbar\Omega_{R0} \cos \omega_d t$ with $\lambda(d^\dagger + d)$, where λ is the coupling between the qubit and driving field, and d, d^\dagger are the annihilation and creation operators of the driving field. The right staircase stands for the dressed states of a driven qubit near resonance, obtained by diagonalizing the corresponding 2×2 Hamiltonian. This yields $|g\rangle = \cos\left(\frac{\pi}{4} - \frac{\beta}{2}\right)|m, \uparrow\rangle + \sin\left(\frac{\pi}{4} - \frac{\beta}{2}\right)|m+1, \downarrow\rangle$ and $|e\rangle = -\sin\left(\frac{\pi}{4} - \frac{\beta}{2}\right)|m, \uparrow\rangle + \cos\left(\frac{\pi}{4} - \frac{\beta}{2}\right)|m+1, \downarrow\rangle$. The bare Rabi frequency is $\Omega_{R0} \approx \lambda\sqrt{\bar{m}}$, where \bar{m} is the average photon number in the coherent (classical) driving field. Red arrows stand for transition rates. In the lab frame at low temperature only the relaxation Γ_\downarrow needs to be considered. However, in the dressed states basis the dominant rate is from the state $|g\rangle$ to the state $|e\rangle$, thus creating an inversion.

we obtain for $\beta = 0$

$$\frac{\tilde{\Gamma}_\downarrow}{\tilde{\Gamma}_\uparrow} = \frac{\langle \hat{X}^2 \rangle_{\omega_d + \Omega_R}}{\langle \hat{X}^2 \rangle_{\omega_d - \Omega_R}}. \quad (14)$$

For example, for Ohmic noise and low bath temperature this reduces to $\tilde{\Gamma}_\downarrow/\tilde{\Gamma}_\uparrow \approx 1 + 2\Omega_R/\omega_d$, which corresponds to an effective temperature of order $2\hbar\omega_d/k_B \approx 2\Delta E/k_B$, which by assumption is high but finite. The infinite temperature threshold is crossed toward negative temperatures at weak blue detuning when the condition

$$\frac{(1 + \sin \beta)^2}{(1 - \sin \beta)^2} \sim 1 + \frac{2\Omega_R}{\omega_d} \quad (15)$$

is satisfied. We note that all qualitative features are well reproduced by the approximation (13).

To illustrate the calculations outlined above and the mechanism creating the population inversion for blue detuning we show in Fig. 3 the level structure, i.e., the formation of dressed states, of a near-resonantly driven qubit. For the purpose of the present discussion we assume that also the driving field is quantized. This level structure was described first by Mollow [17]. The picture also illustrates how for blue detuning a pure relaxation process, Γ_{\downarrow} , in the laboratory frame predominantly leads to an excitation process, $\tilde{\Gamma}_{\uparrow}$, in the rotating frame, thus creating a population inversion in the basis of “dressed states”.

If this effective inverted two-state system is coupled to an oscillator, a lasing state is induced. In Ref. [20] it was proposed to couple the oscillator to the dressed states belonging to the neighboring doublets (see Fig. 3). Then, to be in resonance with the pair of dressed states with population inversion the oscillator frequency should satisfy $\omega_0 = \omega_d + \Omega_R$. As $\omega_d \sim \Delta E$ and $\Omega_R \ll \Delta E$ this can work for a high-frequency resonator approximately in resonance with the qubit, $\omega_0 \approx \Delta E$. In contrast, in Ref. [22] a different situation was considered where the oscillator was coupled to the dressed states belonging to the same doublet. The resonance condition then reads $\omega_0 = \Omega_R$, and the lasing can be reached for an oscillator much slower than the qubit, $\omega_0 \ll \Delta E$, which is the situation realized in Ref. [2]. An additional complication arises at the symmetry point of the qubit, since there the single-photon coupling between the oscillator and the doublet of the dressed states vanishes. Then, two-photon processes become relevant with the resonance condition $2\omega_0 = \Omega_R$ [22].

3. Modelling the few-qubit laser

In this Section we discuss various properties of superconducting micromasers. We use different theoretical approaches depending on the quantity we want to calculate. The presentation of different approximation schemes and the discussion of the physics of the system will thus proceed in parallel.

3.1. The model

We consider a single-mode quantum resonator coupled to N_a qubits (labelled by μ). In the absence of dissipation in the rotating wave approximation the dynamics of the system is described by the Tavis-Cummings Hamiltonian [23]:

$$H_{\text{TC}} = \hbar\omega_0 a^\dagger a + \frac{1}{2}\hbar\epsilon \sum_{\mu} \sigma_z^{\mu} + \hbar g \sum_{\mu} (\sigma_+^{\mu} a + \sigma_-^{\mu} a^\dagger). \quad (16)$$

Here we introduced, apart from the photon annihilation and creation operators, a and a^\dagger , the Pauli matrices acting on the single-qubit eigenstates $\sigma_z^{\mu} = |\uparrow_{\mu}\rangle \langle \uparrow_{\mu}| - |\downarrow_{\mu}\rangle \langle \downarrow_{\mu}|$, $\sigma_+^{\mu} = |\uparrow_{\mu}\rangle \langle \downarrow_{\mu}|$, and $\sigma_-^{\mu} = |\downarrow_{\mu}\rangle \langle \uparrow_{\mu}|$. Including both resonator and qubit dissipation the total Hamiltonian becomes

$$H = H_{\text{TC}} + (a + a^\dagger)X_a + \sum_{\mu} (X_z^{\mu}\sigma_z^{\mu} + X_+^{\mu}\sigma_+^{\mu} + X_-^{\mu}\sigma_-^{\mu}) + H_{\text{bath}}. \quad (17)$$

Dissipation is modeled by assuming that the oscillator and the qubits interact with noise operators, X_a and X_z^μ , X_+^μ , X_-^μ , belonging to independent baths with Hamiltonian H_{bath} in thermal equilibrium [24]. The noise coupling longitudinally to the qubits, $X_z^\mu \sigma_z^\mu$, is responsible for the qubits' pure dephasing.

In this section and beyond we do not describe anymore the detailed mechanism creating the population inversion in the qubits, which is necessary to obtain lasing. Rather we introduce it by assuming that the effective temperature of the qubits' baths is negative. (In the same spirit the transition rates Γ appearing below are those of the effective two-level system, even if they refer to transition between dressed states, for which the rates were denoted above by $\tilde{\Gamma}$.) Possible deviations from the Tavis-Cummings oscillator-qubit coupling used in Eq. (17) are discussed in Appendix A.

3.2. Quantum Langevin equations

From the Hamiltonian (17), working in the Heisenberg picture and following the route described, e.g., in Ref. [14], we derive a set of quantum Langevin equations of motion,

$$\begin{aligned} \frac{d}{dt} \sigma_z^\mu &= -2ig (\sigma_+^\mu a - \sigma_-^\mu a^\dagger) - \Gamma_1 (\sigma_z^\mu - D_0) + F_z^\mu(t) , \\ \frac{d}{dt} \sigma_+^\mu &= -(\Gamma_\varphi - i\epsilon) \sigma_+^\mu - ig \sigma_z^\mu a^\dagger + F_+^\mu(t) , \\ \frac{d}{dt} a &= -\left(\frac{\kappa}{2} + i\omega_0\right) a - ig \sum_\mu \sigma_-^\mu + F_a(t). \end{aligned} \quad (18)$$

Here the rate $\Gamma_1 = \Gamma_\downarrow + \Gamma_\uparrow$ is the sum of excitation and relaxation rates, while $\Gamma_\varphi = \Gamma_1/2 + \Gamma_\varphi^*$ is the total dephasing rate, incl. the “pure dephasing” due to longitudinal noise described by Γ_φ^* . In contrast to relaxation and excitation processes, pure dephasing arises due to processes with no energy exchange between qubit and environment and thus does not affect the populations of the two qubit states. Furthermore, κ is the bare resonator damping. The parameter $D_0 = (\Gamma_\uparrow - \Gamma_\downarrow)/\Gamma_1$ denotes the stationary qubit polarization in the absence of the resonator. In the present case, since we assume a negative temperature of the qubit baths and a population inversion we have $D_0 > 0$.

The Langevin operators $F_i^\mu(t)$ with $i = +, -, z$ have vanishing averages and are characterized by their correlation functions, $\langle F_i^\mu(t) F_j^\nu(t') \rangle = \delta_{\mu\nu} D_{ij}^\mu g_q(t - t')$. The function $g_q(t - t')$ is assumed to decay on a time scale much shorter than the relaxation and decoherence times of the qubits and the oscillator. The diffusion coefficients D_{ij}^μ are related to the rates introduced above, $D_{+-}^\mu = \Gamma_\uparrow + \Gamma_\varphi^* (1 + \langle \sigma_z^\mu \rangle)$, $D_{-+}^\mu = \Gamma_\downarrow + \Gamma_\varphi^* (1 - \langle \sigma_z^\mu \rangle)$, $D_{zz}^\mu = 2\Gamma_1 - 2(\Gamma_\uparrow - \Gamma_\downarrow) \langle \sigma_z^\mu \rangle$, $D_{z+}^\mu = 2\Gamma_\downarrow \langle \sigma_+^\mu \rangle$, $D_{z-}^\mu = -2\Gamma_\uparrow \langle \sigma_-^\mu \rangle$. Similarly, the Langevin force $F_a(t)$ acting on the resonator with $\langle F_a^\dagger(t) F_a(t') \rangle = \kappa N_{\text{th}} g_a(t - t')$ is characterized by the rate κ and thermal photon number N_{th} . The qubit and oscillator noises are assumed to be independent. For a further discussion of the different rates and diffusion coefficients we refer to standard quantum optics textbooks, e.g., Ref. [25].

3.3. Master equation

Alternatively, the dynamics of a single- or few-qubit laser can be analyzed in the frame of a Master equation approach, as discussed by several authors [22, 26, 27, 28, 29]. In the Schrödinger picture the Master equation for the reduced density matrix ρ of the qubits and the oscillator reads

$$\dot{\rho} = -\frac{i}{\hbar} [H_{\text{TC}}, \rho] + L_Q \rho + L_R \rho. \quad (19)$$

The Liouville operators L_R and L_Q describe the resonator's and qubits' dissipative processes. For Markovian processes it is sufficient to approximate them by Lindblad forms,

$$\begin{aligned} L_R \rho = \frac{\kappa}{2} [(N_{\text{th}} + 1) (2a\rho a^\dagger - a^\dagger a \rho - \rho a^\dagger a) \\ + N_{\text{th}} (2a^\dagger \rho a - a a^\dagger \rho - \rho a a^\dagger)] \end{aligned} \quad (20)$$

and

$$\begin{aligned} L_Q \rho = \sum_{\mu} \left[\frac{\Gamma_{\varphi}^*}{2} (\sigma_z^{\mu} \rho \sigma_z^{\mu} - \rho) + \frac{\Gamma_{\downarrow}}{2} (2\sigma_{-}^{\mu} \rho \sigma_{+}^{\mu} - \rho \sigma_{+}^{\mu} \sigma_{-}^{\mu} - \sigma_{+}^{\mu} \sigma_{-}^{\mu} \rho) \right. \\ \left. + \frac{\Gamma_{\uparrow}}{2} (2\sigma_{+}^{\mu} \rho \sigma_{-}^{\mu} - \rho \sigma_{-}^{\mu} \sigma_{+}^{\mu} - \sigma_{-}^{\mu} \sigma_{+}^{\mu} \rho) \right]. \end{aligned} \quad (21)$$

Again the dissipative evolution depends on four rates, Γ_{\uparrow} , Γ_{\downarrow} , Γ_{φ}^* and κ , and on the thermal photon number N_{th} . Differently from the quantum Langevin equations, the Master equation (19) allows us to determine completely the quantum state of the system. However, its full solution is numerically demanding in the experimental regime of parameters due to the high number of photons in the resonator (of the order of 10^2 or higher for a single-qubit laser). In the following we combine both Master equation and quantum Langevin approach to calculate to a good approximation the physically relevant quantities.

4. Approximations and static properties

By taking appropriate products of Eqs. (18) and performing averaging, we arrive at the following equations for the average photon number $\langle n \rangle$, the qubit polarization $\langle \sigma_z^{\mu} \rangle$ and the product $\langle \sigma_{+}^{\mu} a \rangle$,

$$\begin{aligned} \frac{d}{dt} \langle \sigma_z^{\mu} \rangle &= -2ig (\langle \sigma_{+}^{\mu} a \rangle - \langle \sigma_{-}^{\mu} a^{\dagger} \rangle) - \Gamma_1 (\langle \sigma_z^{\mu} \rangle - D_0) \\ \frac{d}{dt} \langle n \rangle &= ig \sum_{\mu} (\langle \sigma_{+}^{\mu} a \rangle - \langle \sigma_{-}^{\mu} a^{\dagger} \rangle) - \kappa (\langle n \rangle - N_{\text{th}}), \\ \frac{d}{dt} \langle \sigma_{+}^{\mu} a \rangle &= (i\Delta - \gamma) \langle \sigma_{+}^{\mu} a \rangle - ig \langle \sigma_z^{\mu} n \rangle - ig \sum_{\nu} \langle \sigma_{+}^{\mu} \sigma_{-}^{\nu} \rangle. \end{aligned} \quad (22)$$

Here we introduced the detuning $\Delta = \epsilon - \omega_0$ and the total dephasing rate $\gamma = \Gamma_{\varphi} + \frac{\kappa}{2}$.

In the stationary limit, after isolating the correlations between different qubits by writing $\langle \sigma_+^\mu \sigma_-^\nu \rangle = \delta_{\mu\nu}(1 + \langle \sigma_z^\mu \rangle) + (1 - \delta_{\mu\nu})\langle \sigma_+^\mu \sigma_-^\nu \rangle$, we derive from the previous equations the following two exact relations between four quantities: the average qubit polarization $\langle S_z(t) \rangle$ with $S_z \equiv \frac{1}{N_a} \sum_\mu \sigma_z^\mu$, the photon number $\langle n(t) \rangle$, and the correlation functions $\langle n S_z \rangle$ and $C_{QQ} = \frac{1}{N_a} \sum_{\mu \neq \nu} \langle \sigma_+^\mu \sigma_-^\nu \rangle$,

$$\begin{aligned} \langle n \rangle &= N_{\text{th}} + \frac{2g^2 N_a}{\kappa} \frac{\gamma}{\gamma^2 + \Delta^2} \left[\langle S_z n \rangle + \frac{1}{2}(\langle S_z \rangle + 1) + C_{QQ} \right], \\ \langle S_z \rangle &= D_0 - \frac{4g^2}{\Gamma_1} \frac{\gamma}{\gamma^2 + \Delta^2} \left[\langle S_z n \rangle + \frac{1}{2}(\langle S_z \rangle + 1) + C_{QQ} \right]. \end{aligned} \quad (23)$$

If two of them are known, e.g., from a numerical solution of the Master equation, the other two can readily be determined.

4.1. Semi-quantum model

Factorizing the correlator, $\langle S_z n \rangle \approx \langle S_z \rangle \langle n \rangle$, on the right-hand side of Eqs. (23) and neglecting the qubit-qubit correlations, $C_{QQ} \simeq 0$, we reproduce results known in quantum optics as “semi-quantum model” [16]. This approximation yields a quadratic equation for the scaled average photon number (per qubit) $\tilde{n} = \langle n \rangle / N_a$,

$$\begin{aligned} \tilde{n}^2 + \left(\tilde{n}_0 - \frac{\Gamma_1 D_0}{2\kappa} - \frac{N_{\text{th}}}{N_a} + \frac{1}{2N_a} \right) \tilde{n} + \\ - \left(\frac{N_{\text{th}} \tilde{n}_0}{N_a} + \frac{N_{\text{th}}}{2N_a^2} + \frac{\Gamma_1 D_0 + 1}{4\kappa} \frac{1}{N_a} \right) = 0, \end{aligned} \quad (24)$$

which depends on the parameter $\tilde{n}_0 = \frac{\Gamma_1 \gamma}{4g^2 N_a} \left(1 + \frac{\Delta^2}{\gamma^2} \right)$. This equation has always one positive solution $\tilde{n} > 0$.

4.2. Semiclassical approach

Before entering the analysis of the properties of the semi-quantum solution, for sake of comparison, we recall the standard semiclassical results. In the semi-classical approximation, the operator a is treated as a classical stochastic variable, α . In this case, after adiabatic elimination of the qubits’ degrees of freedom, i.e., assuming $\Gamma_\varphi \gg \kappa/2$, one obtains from Eqs. (18) a classical Langevin equation for α ,

$$\dot{\alpha} = - \left[\frac{\kappa}{2} - \frac{g^2 N_a}{\Gamma_\varphi - i\Delta} s_z^{\text{st}} \right] \alpha + \xi(t), \quad (25)$$

where $\xi(t)$ is a classical Langevin force due to thermal noise, $\langle \xi(t) \xi^*(t') \rangle = \kappa N_{\text{th}} \delta(t - t')$, and $s_z^{\text{st}} = D_0 / (1 + |\alpha|^2 / (\tilde{n}_0 N_a))$ denotes the stationary qubits’ polarization.

In order to obtain an expression for the average photon number $\langle n \rangle = \langle |\alpha|^2 \rangle$ we rewrite the Langevin equation as $\dot{\alpha} = -f(|\alpha|^2)\alpha + \xi(t)$ and approximate $\langle f(|\alpha|^2) \cdot |\alpha|^2 \rangle \approx f(\langle n \rangle) \cdot \langle n \rangle$. Thus we arrive at the equation $\frac{d}{dt} \langle n \rangle = -2\text{Re}\{f(\langle n \rangle)\} \cdot \langle n \rangle + \kappa N_{\text{th}}$, from

which we obtain in the steady state a quadratic equation for the scaled photon number $\tilde{n} = \langle n \rangle / N_a$,

$$\tilde{n}^2 + \left(\tilde{n}_0 - \frac{\Gamma_1 D_0}{2\kappa} - \frac{N_{\text{th}}}{N_a} \right) \tilde{n} - \frac{N_{\text{th}} \tilde{n}_0}{N_a} = 0 \quad (26)$$

In the zero temperature limit, $N_{\text{th}} \sim 0$, the semiclassical results can be rewritten in the simple form, $\tilde{n}^2 + (\tilde{n}_0 - \Gamma_1 D_0 / 2\kappa) \tilde{n} \approx 0$, which gives the well-known threshold condition: $D_0 = \kappa\gamma / (2g^2 N_a)$.

4.3. Comparison of the different approaches

Different from the semiclassical picture, the semi-quantum model includes the effects of spontaneous emission processes, described by the term proportional to $(\langle S_z \rangle + 1)$ in Eqs. (23). Spontaneous emission is responsible for the linewidth of the lasers, and, as noticed in Ref. [27], due to the low photon number, spontaneous emission is especially relevant for the dynamics of single-atom lasers.

To illustrate the effect of spontaneous emission on the lasing transition and at the same time the quality of the semi-quantum approximation, we plot the photon number as a function of the coupling strength g for $N_a = 1$ (Fig. 4a) and $N_a = 2$ (Fig. 4b). The plots show the semi-quantum, semi-classical and Master equation results. We note that the semi-quantum approximation gives results in very good agreement with the Master equation. Moreover, both the semi-quantum and Master equation solution show a smooth crossover between the normal and the lasing regimes, an effect which is due to spontaneous emission. While we cannot define a sharp threshold condition, we can still identify, even for a single-atom laser, a well localized transition region centered at the threshold coupling predicted by the semiclassical approximation.

In Fig. 4a we also plot the qubit-oscillator correlator, $\langle S_z n \rangle$, and the factorized approximation, $\langle S_z \rangle \langle n \rangle$. For strong coupling, both differ significantly. However, as the good agreement between the semi-quantum approximation and the numerical solution of the Master equation demonstrates, the qubit-field correlations have only a weak effect on the average photon number. On the other hand, as we will see in the following section, the qubit-field correlations have an important effect on the spectral properties of the single-qubit laser.

Fig. 4b shows the qubit-qubit correlations C_{QQ} for a two-qubit-laser. Similar as the qubit-field correlations, they are neglected in the semi-quantum approximation. Both correlations are maximum at the lasing transition, but decay away from this point. The reason is that qubit-field and qubit-qubit correlations scale as g^2 / Γ_φ^2 , thus they are small for weak coupling. On the other hand, they are proportional to the qubit inversion $\langle S_z \rangle$ and hence vanish rapidly above the transition.

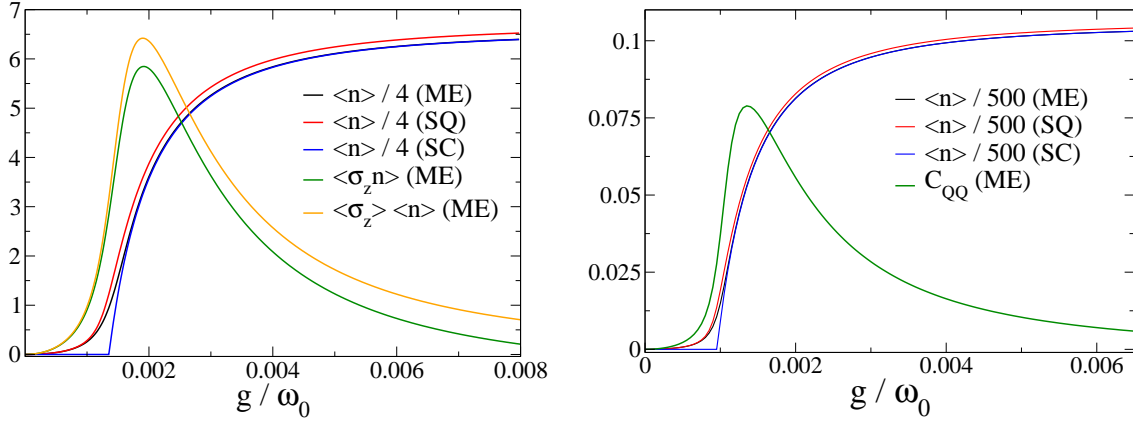


Figure 4. (a) Average photon number $\langle n \rangle$ in the resonator and qubit-field correlations for a single-qubit-laser. The photon number is calculated using the Master equation (ME, black line), the semi-quantum (SQ, red line), and the semi-classical approximation (SC, blue line). The green and orange line show the average values $\langle \sigma_z n \rangle$ and $\langle \sigma_z \rangle \langle n \rangle$. (b) Average photon number $\langle n \rangle$ in the resonator and qubit-qubit correlations C_{QQ} (green line) for a two-qubit-laser. The photon number was calculated using the Master equation (black line), the semi-quantum (red line), and the semi-classical approximation (blue line). The parameters are $\epsilon = \omega_0$, $\Gamma_1 / \omega_0 = 0.016$, $\Gamma_\varphi^* / \omega_0 = 0.004$, $D_0 = 0.975$, $\kappa / \omega_0 = 3 \cdot 10^{-4}$, and $N_{\text{th}} = 0$.

5. Spectral properties

For typical circuit QED parameters, i.e., for strong coupling g , the semi-quantum approximation, in spite of giving a sufficient estimate of the stationary photon number, cannot be used for a quantitative study of spectral functions. On the other hand, the Master equation is hard to solve in the time-dependent case. For the analysis of phase diffusion we thus proceed in a hybrid approach: starting from Heisenberg equations of motion we derive analytical expressions for the phase diffusion rate and frequency shift in terms of single-time averages as the photon number and the qubit inversion in the stationary state. We then use the Master equation for the reduced qubit-resonator density matrix to calculate these single-time averages.

We want to analyze the laser and cross correlation functions, $O(\tau)$ and $G(\tau)$,

$$\begin{aligned} O(\tau) &= \lim_{t \rightarrow \infty} \langle a^\dagger(t + \tau) a(t) \rangle, \\ G(\tau) &= \lim_{t \rightarrow \infty} \langle S_+(t + \tau) a(t) \rangle, \end{aligned} \quad (27)$$

where $S_+ = \frac{1}{N_a} \sum_\mu \sigma_+^\mu$. Starting from the quantum Langevin equations (18), we derive a hierarchy of equations involving $O(\tau)$ and $G(\tau)$:

$$\begin{aligned} \frac{d}{d\tau} O(\tau) &= \left(i\omega_0 - \frac{\kappa}{2} \right) O(\tau) + ig N_a G(\tau), \\ \frac{d}{d\tau} G(\tau) &= (i\epsilon - \Gamma_\varphi) G(\tau) - ig \langle S_z(t + \tau) a^\dagger(t + \tau) a(t) \rangle. \end{aligned} \quad (28)$$

Instead of factorizing $\langle S_z(t + \tau)a^\dagger(t + \tau)a(t) \rangle \approx \langle S_z \rangle \langle a^\dagger(t + \tau)a(t) \rangle$, which would correspond to the semi-quantum approach, we use the following approximation:

$$\langle S_z(t + \tau)a^\dagger(t + \tau)a(t) \rangle \simeq \frac{1}{2} \left(\langle S_z \rangle + \frac{\langle S_z n \rangle}{\langle n \rangle} \right) \langle a^\dagger(t + \tau)a(t) \rangle \quad (29)$$

This factorization is explained in detail in Appendix B. It allows us to account for qubit-oscillator correlations $\langle \delta S_z(t) \delta n(t) \rangle = \langle S_z n \rangle - \langle S_z \rangle \langle n \rangle$, which become important above the lasing transition, i.e., for strong coupling, when the qubit inversion tends to zero, $\langle S_z \rangle \rightarrow 0$.

We now get a closed set of equations for the correlation functions $O(\tau)$ and $G(\tau)$,

$$\begin{aligned} \frac{d}{d\tau} O(\tau) &= \left(i\omega_0 - \frac{\kappa}{2} \right) + igN_a G(\tau), \\ \frac{d}{d\tau} G(\tau) &= (i\epsilon - \Gamma_\varphi) G(\tau) - \frac{ig}{2} \left(\langle S_z \rangle + \frac{\langle S_z n \rangle}{\langle n \rangle} \right) O(\tau). \end{aligned} \quad (30)$$

We focus on the case where the oscillator damping is much weaker than the qubits' dephasing, $\kappa/2 \ll \Gamma_\varphi$, which is usually satisfied in single-qubit lasing experiments. In this case we obtain from (30) a Lorentzian spectral function for the oscillator

$$\hat{O}(\omega) = \frac{2\kappa_d \langle n \rangle}{(\omega - \omega_0 - \delta\omega_0)^2 + \kappa_d^2} \quad (31)$$

where $\hat{O}(\omega)$ denotes the Fourier transform of $O(\tau)$.

By combining Eqs. (30) and (23), the phase diffusion rate, κ_d , and the frequency shift, $\delta\omega_0$, can be cast in the following form:

$$\begin{aligned} \kappa_d &= \frac{\kappa N_{\text{th}}}{2 \langle n \rangle} + \frac{g^2 N_a \Gamma_\varphi (\langle S_z \rangle + 1)}{2 \langle n \rangle \Gamma_\varphi^2 + \Delta^2} \\ &\quad + \frac{g^2 N_a \Gamma_\varphi}{\Gamma_\varphi^2 + \Delta^2} \frac{\langle S_z n \rangle - \langle S_z \rangle \langle n \rangle}{2 \langle n \rangle} + \frac{g^2}{\langle n \rangle} \frac{\Gamma_\varphi}{\Gamma_\varphi^2 + \Delta^2} \sum_{\mu, \nu}^{\mu \neq \nu} \langle \sigma_+^\mu \sigma_-^\nu \rangle, \end{aligned} \quad (32)$$

and

$$\begin{aligned} \delta\omega_0 &= \frac{\Delta}{2 \langle n \rangle} \left[\frac{\kappa(\langle n \rangle - N_{\text{th}})}{\Gamma_\varphi} - g^2 N_a \frac{(\langle S_z \rangle + 1)}{\Gamma_\varphi^2 + \Delta^2} \right] \\ &\quad - \frac{g^2 N_a \Delta}{\Gamma_\varphi^2 + \Delta^2} \frac{\langle S_z n \rangle - \langle S_z \rangle \langle n \rangle}{2 \langle n \rangle} + \frac{g^2}{\langle n \rangle} \frac{\Delta}{\Gamma_\varphi^2 + \Delta^2} \sum_{\mu, \nu}^{\mu \neq \nu} \langle \sigma_+^\mu \sigma_-^\nu \rangle. \end{aligned} \quad (33)$$

Upon factorization of the correlator $\langle S_z n \rangle$ above and below threshold, Eqs. (32) and (33) reduce to results known from quantum optics [14]. The phase diffusion rate (32) is the sum of four terms. The first represents a thermal contribution to the linewidth and is negligible in the regime explored in [12]. The second describes the effect of spontaneous emission of the qubit, which, due to the strong coupling, strongly increases the linewidth. These first two terms correspond to the semi-quantum approximation. While not giving a quantitatively correct description of the spectral properties, they catch the most relevant qualitative features, both below and above the transition to the lasing regime.

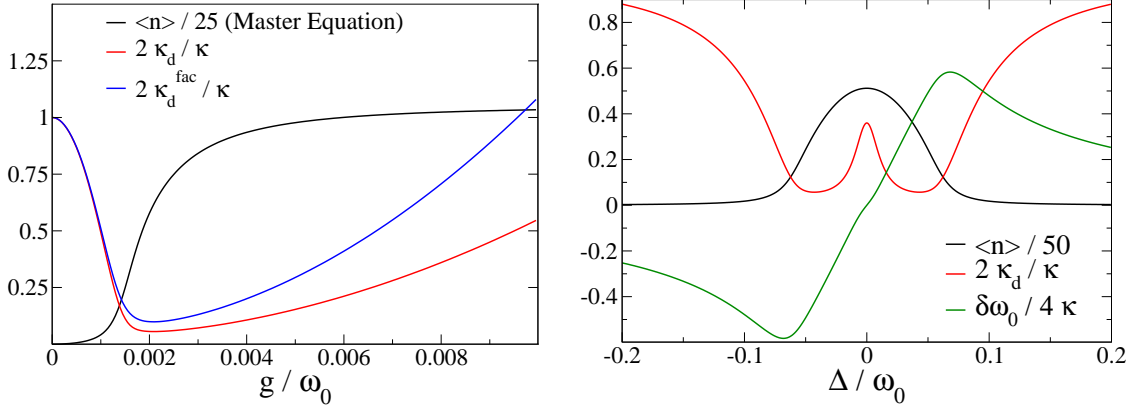


Figure 5. Left panel: Phase diffusion constant and average photon number (black line) as a function of the coupling strength g for a single-qubit laser. The phase diffusion constant is calculated using the hybrid approach (red line) and the semi-quantum approximation (blue line). Right panel: Phase diffusion constant (red line), frequency shift (green line) and photon number (black line) as a function of the detuning for a fixed coupling strength $g/\omega_0 = 0.008$. Other parameters as in Figure 4.

The third term, due to qubit-field correlations, is essentially a measure of the coherent coupling between the qubit and the oscillator. As we will see, it gives a significant quantitative contribution to the linewidth as well as to the frequency shift. The fourth term due to qubit-qubit correlations is very small and can be neglected in the typical experimental regime.

For the following discussion we focus on the case of a single qubit, $N_a = 1$. In Fig. 5 we plot the diffusion constant κ_d (32), as function of the coupling strength g , covering the whole range from below to above the transition, and compare it to the diffusion constant κ_d^{fac} , obtained by factorizing the correlator $\langle \sigma_z n \rangle$ and neglecting C_{QQ} . Upon approaching the broadened lasing threshold from the weak coupling side we observe the linewidth narrowing characteristic for the lasing transition. However, above the transition the linewidth increases again with growing coupling strength, thus deteriorating the lasing state. We also observe that qubit-oscillator correlations have a significant quantitative effect on the phase diffusion and lead to a *reduction* of the linewidth.

In Fig. 5 we also note that in the transition region there is an “optimal” value of the qubit-oscillator coupling where the height of the spectral line, which is given by the ratio photon number to phase diffusion is maximum. This interesting feature is due to the fact that in single- and few-qubit lasers far above the lasing transition a reduction of the coupling has little effect on the saturated photon number but leads to a decrease of the incoherent photon emission rate, thus diminishing the linewidth. Another manifestation of this effect can be seen in Fig. 5 (right panel) where we plotted the photon number, the phase diffusion constant and the frequency shift as a function of the detuning, Δ between qubit and oscillator.

Here we observe, that while, due to the strong coupling, the photon number is

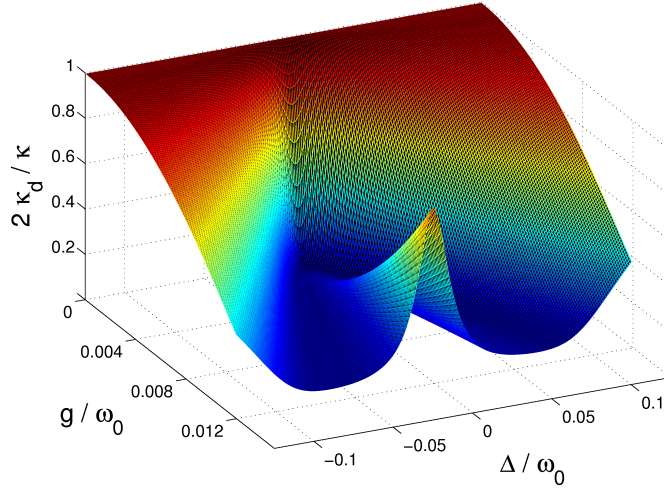


Figure 6. Phase diffusion rate κ_d for a single-qubit laser as a function of the detuning Δ and the coupling strength g . Other parameters as in Figure 4.

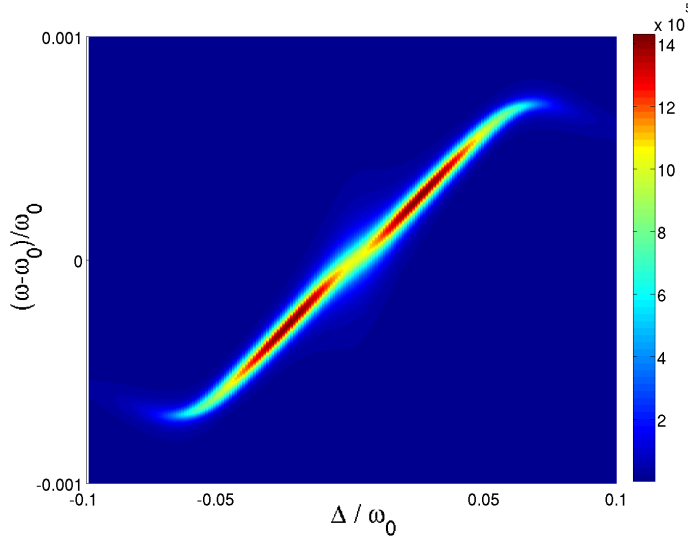


Figure 7. Emission spectrum $S(\omega)$ as a function of the detuning Δ for a fixed coupling strength $g/\omega_0 = 0.006$. Other parameters as in Figure 4. The spectrum has been artificially broadened to make the double-peak structure better visible.

roughly constant in a wide region around $\Delta = 0$, the phase diffusion constant shows a double minimum structure.

The same behavior can be observed in Fig. 6 where we plot the phase diffusion rate κ_d as a function of the detuning Δ and the coupling strength g . We see that the optimal lasing conditions are realized somewhat out of resonance, where the effective coupling is weaker. In the region of strong coupling, we thus observe two peaks symmetrically shifted with respect to $\Delta = 0$ in the emission spectrum, as shown in Fig. 7. A similar

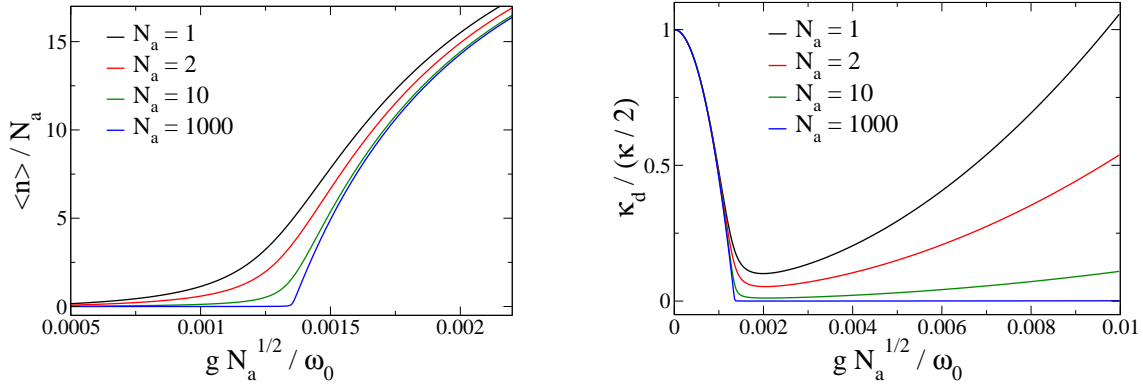


Figure 8. Average scaled photon number and phase diffusion constant as a function of the scaled coupling $g\sqrt{N_a}$. Other parameters as in Figure 4.

structure in the output spectrum of single atom lasers was also found in a numerical study by Ginzler *et al.* [28]. One might conjecture that this effect is the origin of the two spots ‡ observed in the experiments of Astafiev *et al.* [12]. It would explain why the peaks do not occur at resonance, but we have not succeeded to fit the experimental data in a satisfactory way. In the paper reporting the experiments it was proposed that the second peak is related to two-photon processes. Indeed extensions of the model Eq. (17) contain an effective two photon-coupling between the qubit and the resonator. However, as described in the Appendix, the two-photon coupling constant appears to be too small to produce any “two-photon lasing”. This results is also confirmed by the numerical solution of the Master equation. We also note that in the experiment the second peak appears substantially shifted from the two-photon resonance condition. Using the data of Ref. [12], at the second peak we have $2\omega_0 - \epsilon \simeq 0.4\omega_0$.

6. Discussion

6.1. Scaling in the semi-quantum approximation

As discussed in a quantum optics context in Refs. [27, 28], various properties of single qubit masers are due to the fact that in these systems only one artificial atom (a *microscopic* system from a thermodynamical point of view) interacts with the electromagnetic radiation. To clarify the main differences between single qubit masers and conventional (many atom) lasers, we use the semi-quantum approximation to study the scaling of the average photon number and of the phase diffusion with the number

‡ In Ref. [12], Astafiev *et al.* study the resonator spectrum as a function of the charging energy of the SSET and observe two bright spots, blue and red detuned with respect to the $\Delta = 0$ condition. We remark, that since in the experiment the Josephson energy is kept constant the detuning depends monotonically on the charging energy. Moreover a variation of the charging energy not only changes the detuning but also the coupling and the inversion. This does not change substantially the structure of the spectrum, but it leads to asymmetries between two peaks.

of atoms.

In Fig. 8, we plot the scaled photon number $\langle n \rangle / N_a$ in the transition region and κ_d versus the scaled coupling, $g\sqrt{N_a}$, for different values of the number of qubits N_a . Plotting these scaled values all curves have the same asymptotic behavior and the transition occurs at the same position. As expected, in Fig. 8 (left panel) we observe that for low values of N_a , there is a smoothening of the lasing transition which is due to spontaneous emission processes and disappears in the large N_a limit. In Fig. 8 (right panel) we show the scaling of the phase diffusion constant. Here the qubits' relaxation processes are responsible for the increase of the phase diffusion rate in the case of strong qubit-oscillator coupling for small N_a .

6.2. Effect of the low-frequency noise

The linewidth of order of 0.3MHz observed in Ref. [12] is about one order of magnitude larger than what follows from Eq. (32) (of the order of the Schawlow-Townes linewidth). Moreover, in the experiment, the emission line shows a Gaussian rather than a Lorentzian shape. Both discrepancies may be explained if we note that the qubits' dephasing is mostly due to low-frequency charge noise, which cannot be treated within the Markov approximation used in the derivation of Eqs.(32)-(33).

However, low-frequency (quasi-static) noise can be taken into account by averaging the Lorentzian line in Eq. (32) over different values of the energy splitting ϵ of the qubit [30], or equivalently, over different values of the detuning Δ between qubit and oscillator. Assuming that these fluctuations are Gaussian distributed, with mean $\bar{\Delta}$ and width σ , such that $\Gamma_1 > \sigma \gg \kappa_d$, we can neglect in the saturated limit the dependence of κ_d and $\langle n \rangle$ on Δ and assume that the frequency shift $\delta\omega_0$ depends linearly on the detuning Δ .

From Eq. (33) we then have $\delta\omega_0 \simeq \Delta\kappa/(2\Gamma_\varphi)$, and we obtain a Gaussian line of width $\tilde{\sigma} \simeq \sigma\kappa/(2\Gamma_\varphi)$, where we remark that Γ_φ is the total *Markovian* dephasing rate. In this way, the linewidth observed in the experiment can be reproduced by a reasonable choice of σ of order of 300 MHz. In the case in which σ is larger than Γ_1 , the previous formula overestimates the linewidth since it does not take into account the decay of $\langle n \rangle$ below the lasing transition. In this case we can still perform the averaging numerically. In either case we note that in the presence of low-frequency noise, the linewidth is governed not by κ_d , but by $\delta\omega_0$.

7. Conclusions

We analyzed in detail the static and spectral properties of single- and few-qubit lasers. Our main conclusions are:

- As compared to a conventional laser setup with many atoms, which has a sharp transition to the lasing state at a threshold value of the coupling strength (or inversion), we find for a single- or few-qubit laser a smeared transition. But it is still well pronounced. Similarly, the decrease of the phase diffusion strength with increasing

coupling below the transition, which leads to the characteristic linewidth narrowing, is less sharp but still pronounced.

- Above the lasing transition we observe for a single- or few-qubit laser a pronounced increase of the phase diffusion strength, not observed for conventional lasers, which leads to a deterioration of the lasing state.
- Due to the strong coupling between the qubits and the oscillator, nontrivial structures appear in the spectrum, which are not visible in the average photon number. As shown in Fig. 6 the optimal lasing conditions are realized for two values of the detuning, which are symmetrically shifted from the resonance $\Delta = 0$. At these two hot-spots the output spectrum has the maximum height, and it is centered around the shifted frequency $\omega_0 \pm \delta\omega_0$.
- Low-frequency noise strongly affects the line shape of the two peaks, leading to an inhomogeneous broadening. In comparison, the natural laser linewidth due to spontaneous emission is negligible.

Acknowledgments

We acknowledge fruitful discussions with O. Astafiev and A. Fedorov. The work is part of the EU IST Project EuroSQIP.

Appendix A. Comment on two-photon processes

Here we briefly discuss the validity of the Jaynes-Cummings model introduced in Section 3, when applied to describe the SSET laser of Astafiev *et al.* [12]. As discussed in Section 2.1, the SSET laser, schematically depicted in Fig. 1, consists of a biased superconducting island coupled capacitively to a single-mode electrical resonator. Under appropriate conditions only two charge states, corresponding to $N = 0, 2$ are relevant to the dynamics of the device. In this basis the hamiltonian of the oscillator and the qubit can be written as

$$H = \frac{1}{2} (\epsilon_{ch} \tau_z + E_J \tau_x) + \hbar\omega_0 a^\dagger a - \hbar g_0 \tau_z (a + a^\dagger). \quad (\text{A.1})$$

where the operators τ_x and τ_z are defined as: $\tau_z = (|N=2\rangle\langle N=2| - |N=0\rangle\langle N=0|)$ and $\tau_x = (|N=2\rangle\langle N=0| + |N=0\rangle\langle N=2|)$. Rotating to the qubit's eigenbasis $\{| \uparrow \rangle, | \downarrow \rangle\}$, defined by Eqs. (1), we can recast the hamiltonian as follows:

$$H = \frac{1}{2} \epsilon \sigma_z + \hbar\omega_0 a^\dagger a - \hbar g_0 (\cos \xi \sigma_z - \sin \xi \sigma_x) (a + a^\dagger). \quad (\text{A.2})$$

The angle ξ is defined as in Section 2.1, $\tan \xi = \frac{E_J}{\epsilon_{ch}}$, and the qubit energy splitting, ϵ , depends on the charging and Josephson energies, ϵ_{ch} and E_J : $\epsilon = \sqrt{\epsilon_{ch}^2 + E_J^2}$. In order to identify the one- and two-photon coupling strength, we now apply a Schrieffer-Wolff transformation $U = e^{iS}$ with $S = i \frac{g_0 \cos \xi}{\omega_0} \sigma_z (a - a^\dagger)$ and perform a perturbation

expansion in the parameter g_0/ω_0 . The transformed Hamiltonian, $\tilde{H} = U^\dagger H U$, thus becomes

$$\tilde{H} \simeq \frac{1}{2}\epsilon \sigma_z + \hbar\omega_0 a^\dagger a + \hbar g_1 \sigma_x (a + a^\dagger) + \hbar g_2 i \sigma_y (a^2 - (a^\dagger)^2). \quad (\text{A.3})$$

Here we neglected terms of order $(g_0/\omega_0)^3$ and introduced the two coupling constants $g_1 = -g_0 \sin \xi$ and $g_2 = \frac{2g_0^2}{\omega_0} \sin \xi \cos \xi$ for one-photon and two-photon transitions, respectively. For the parameters used in the experiment the coupling g_2 is roughly two orders of magnitude smaller than the one-photon coupling and below the semiclassical threshold for the two-photon lasing, $g_2^{\text{thr}} = \sqrt{\kappa^2 \Gamma_\varphi / (\Gamma_1 D_0^2)}$ [31]. In the parameter regime explored in the experiments, the Hamiltonian used in Eq. (17) gives thus a good description of the dynamics of the system.

Appendix B. Factorization scheme

The aim of this section is to motivate the approximations and the factorization scheme used in Section 5. The first step is to separate the photon creation and annihilation operators, a and a^\dagger , into an amplitude and a phase: $\langle a^\dagger(t + \tau) a(t) \rangle = \langle \sqrt{n(t + \tau)} (e^{i\varphi(t + \tau)})^\dagger e^{i\varphi(t)} \sqrt{n(t)} \rangle$, where the operator $e^{i\varphi}$ is defined by the expansion: $e^{i\varphi} = \sum_n |n\rangle \langle n + 1|$. Next we write the photon number operator as a sum of a constant and a fluctuating term, $n(t) = \langle n \rangle + \delta n(t)$. In the following we assume that the photon number fluctuations are small, $\sqrt{\delta n^2} \ll \langle n \rangle$. This condition is satisfied above threshold and allows us make the expansion $\sqrt{n(t)} \simeq \sqrt{\langle n \rangle} \left(1 + \frac{\delta n}{2\langle n \rangle} \right)$. Using this expansion we obtain: $\langle a^\dagger(t + \tau) a(t) \rangle \approx \langle n \rangle \langle (e^{i\varphi(t + \tau)})^\dagger e^{i\varphi(t)} \rangle$.

We proceed in a similar way to evaluate the qubit-oscillator correlation function $\langle S_z(t + \tau) a^\dagger(t + \tau) a(t) \rangle$, but, unlike for the oscillator correlation function, here we do not neglect number fluctuations completely. Specifically, we take qubit-oscillator correlations $\langle \delta S_z(t + \tau) \delta n(t + \tau) \rangle = \langle S_z n \rangle - \langle S_z \rangle \langle n \rangle$ into account. The reason for this is that, in general, the condition $|\langle \delta S_z \delta n \rangle| \ll \langle S_z \rangle \langle n \rangle$ is not fulfilled, because the qubit inversion tends to zero above threshold, i.e., for strong coupling: $\langle S_z \rangle \rightarrow 0$.

On the other hand, the correlation function $\langle \delta S_z(t + \tau) \delta n(t) \rangle$ can be shown to decay fast (compared to the typical timescale $\sim 1/\kappa$ of the oscillator) and can be neglected, so that only qubit-oscillator correlations at equal times are kept. This leads us to the equation $\langle S_z(t + \tau) a^\dagger(t + \tau) a(t) \rangle \approx \left(\langle S_z \rangle + \frac{1}{2} \frac{\langle \delta S_z(t) \delta n(t) \rangle}{\langle n \rangle} \right) \langle n \rangle \langle (e^{i\varphi(t + \tau)})^\dagger e^{i\varphi(t)} \rangle$. Eventually, using the relation $\langle \delta S_z(t + \tau) \delta n(t + \tau) \rangle = \langle S_z n \rangle - \langle S_z \rangle \langle n \rangle$ and the above equation for $\langle a^\dagger(t + \tau) a(t) \rangle$, we get our result

$$\langle S_z(t + \tau) a^\dagger(t + \tau) a(t) \rangle \approx \frac{1}{2} \left(\langle S_z \rangle + \frac{\langle S_z n \rangle}{\langle n \rangle} \right) \langle a^\dagger(t + \tau) a(t) \rangle. \quad (\text{B.1})$$

Finally, we remark that the inclusion of the term $\langle S_z n \rangle$ becomes important when the qubit inversion tends to zero, which happens above the lasing threshold. Below threshold, when the qubit inversion is large and correlations are small, the semi-quantum approximation is sufficient for the calculation of the spectral properties.

References

- [1] A. Blais *et al.*, Phys. Rev. A **69**, 062320 (2004); R. Schoelkopf and S. Girvin, Nature **451**, 664 (2008).
- [2] E. Il'ichev *et al.*, Phys. Rev. Lett. **91**, 097906 (2003).
- [3] A. Wallraff *et al.*, Nature **431**, 162 (2004).
- [4] I. Chiorescu *et al.*, Nature **431**, 159 (2004).
- [5] G. Johansson, L. Tornberg, and C. M. Wilson, Phys. Rev. B **74**, 100504 (2006).
- [6] M. A. Sillanpää, J. I. Park, and R. W. Simmonds, Nature **449**, 438 (2007); J. Majer *et al.*, Nature **449**, 443 (2007).
- [7] P.J. Leek *et al.*, Science **318**, 1889 (2007).
- [8] S. Filipp *et al.*, Phys. Rev. Lett. **102**, 200402 (2009); P.J. Leek *et al.*, Phys. Rev. B **79**, 180511(R) (2009).
- [9] L. Di Carlo *et al.*, Nature **460**, 240 (2009).
- [10] M. Hofheinz *et al.*, Nature **454**, 310 (2008); J. M. Fink *et al.*, Nature **454**, 315 (2008).
- [11] M. A. Sillanpää *et al.*, arxiv: 0904.2553 (2009).
- [12] O. Astafiev *et al.*, Nature **449**, 588 (2007).
- [13] M. Grajcar *et al.*, Nature Physics **4**, 612 (2008).
- [14] H. Haken, *Laser Theory*, Springer, Berlin, 1984.
- [15] S. André *et al.*, Phys. Rev. A. **79**, 053848 (2009)
- [16] P. Mandel, Phys. Rev. A **21**, 2020 (1980).
- [17] B. R. Mollow, Phys. Rev. **188**, 1969 (1969).
- [18] F. Bloch, Phys. Rev. **105**, 1206 (1957).
- [19] A. G. Redfield, IBM J. Res. Dev. **1**, 19 (1957).
- [20] J. Zakrzewski, M. Lewenstein, and T. W. Mossberg, Phys. Rev. A **44**, 7717 (1991).
- [21] G. Ithier *et al.*, Phys. Rev. B **72**, 134519 (2005).
- [22] J. Hauss *et al.*, Phys. Rev. Lett. **100**, 037003 (2008).
- [23] M. Tavis and F.W. Cummings, Phys. Rev. **170**, 379 (1968).
- [24] C. W. Gardiner and P. Zoller, *Quantum Noise*, Springer, Berlin, 2004.
- [25] C. Cohen-Tannoudji, J. Dupont-Roc, and G. Grynberg, *Atom-Photon Interactions*, (Wiley, New York, 1992).
- [26] S. Ashhab *et al.*, New J. Phys. **11**, 023030 (2009)
- [27] Y. Mu and C.M. Savage, Phys. Rev. A **46**, 5944 (1992).
- [28] C. Ginzler *et al.*, Phys. Rev. A **48**, 732 (1993).
- [29] D.A. Rodrigues, J. Imbers, and A.D. Armour, Phys. Rev. Lett. **98**, 067204 (2007).
- [30] G. Falci *et al.*, Phys. Rev. Lett. **94**, 167002 (2005).
- [31] Z. C. Wang and H. Haken, Z. Phys. B **55**, 361 (1984).